Journal of Physics D: Applied Physics

PAPER • OPEN ACCESS

Nernst–Planck–Poisson analysis of electrolyte-gated organic field-effect transistors

To cite this article: Najmeh Delavari *et al* 2021 *J. Phys. D: Appl. Phys.* **54** 415101

View the article online for updates and enhancements.

IOP ebooks™

Bringing together innovative digital publishing with leading authors from the global scientific community.

Start exploring the collection–download the first chapter of every title for free.

This content was downloaded from IP address 130.236.82.193 on 15/09/2021 at 08:56

OPEN ACCESS
IOP Publishing

Journal of Physics D: Applied Physics

J. Phys. D: Appl. Phys. 54 (2021) 415101 (11pp)

https://doi.org/10.1088/1361-6463/ac14f3

Nernst–Planck–Poisson analysis of electrolyte-gated organic field-effect transistors

Najmeh Delavari[1], Klas Tybrandt[1], Magnus Berggren[1], Benoît Piro[2], Vincent Noël[2], Giorgio Mattana[2,*] and Igor Zozoulenko[1,*]

[1] Laboratory of Organic Electronics, ITN, Linköping University, 601 74 Norrköping, Sweden
[2] Université de Paris, ITODYS, CNRS, F-75006 Paris, France

E-mail: giorgio.mattana@u-paris.fr and igor.zozoulenko@liu.se

Received 5 February 2021, revised 9 July 2021
Accepted for publication 15 July 2021
Published 29 July 2021

Abstract

Electrolyte-gated organic field-effect transistors (EGOFETs) represent a class of organic thin-film transistors suited for sensing and biosensing in aqueous media, often at physiological conditions. The EGOFET device includes electrodes and an organic semiconductor channel in direct contact with an electrolyte. Upon operation, electric double layers are formed along the gate-electrolyte and the channel-electrolyte interfaces, but ions do not penetrate the channel. This mode of operation allows the EGOFET devices to run at low voltages and at a speed corresponding to the rate of forming electric double layers. Currently, there is a lack of a detailed quantitative model of the EGOFETs that can predict device performance based on geometry and material parameters. In the present paper, for the first time, an EGOFET model is proposed utilizing the Nernst-Planck-Poisson equations to describe, on equal footing, both the polymer and the electrolyte regions of the device configuration. The generated calculations exhibit semi-qualitative agreement with experimentally measured output and transfer curves.

Supplementary material for this article is available online

Keywords: Nernst-Planck-Poisson equations, electrolyte-gated organic field-effect transistors (EGOFET), organic electronics, device modelling

(Some figures may appear in colour only in the online journal)

1. Introduction

Electrolyte-gated organic field-effect transistors (EGOFETs) are organic thin film transistors where the solid-state dielectric, which separates the gate electrode from the organic semiconductor in Organic Field-Effect Transistors (OFETs), is replaced by an electrolyte either in liquid or gel form [1]. In EGOFETs, the application of a gate voltage induces the formation of two Electrical Double Layers (ELDs), one located at the gate/electrolyte interface and the other one at the electrolyte/organic semiconductor thin film interface; the latter is responsible for the accumulation and depletion of mobile electronic charges along the organic semiconductor surface, reversibly switching the channel electrical surface conductivity which thus provides the desired transistor operation [2]. The overall capacitive coupling between the gate electrode and the organic semiconductor can thus be described, to a first approximation, as a series of two capacitors, each associated to the aforementioned interfaces [3]. The values of the two capacitances are inversely proportional to the thicknesses of the two EDL (the so-called Debye lengths), which typically are

* Authors to whom any correspondence should be addressed.

Original content from this work may be used under the terms of the Creative Commons Attribution 4.0 licence. Any further distribution of this work must maintain attribution to the author(s) and the title of the work, journal citation and DOI.

 © 2021 The Author(s). Published by IOP Publishing Ltd Printed in the UK

of a few nm, and proportional to the areas of the two interfaces, respectively. Therefore, in EGOFETs the gate capacitance per unit area (up to 100 $M\mathrm{f\,cm^{-2}}$) [4] is several orders of magnitude higher than those commonly reported for the solid-state dielectrics, traditionally employed in OFETs. As a consequence, the biasing voltages necessary to polarise EGOFETs are typically very small (<1 V) [5].

The intrinsic presence of an electrolyte within their structure, combined with the low biasing voltages, make EGOFETs ideal candidates for the next generation of sensors and biosensors working in liquid environments [6]. Indeed, several examples of EGOFET-based biosensors have recently been reported for the detection of a wide variety of biologically relevant molecules, such as: DNA [7], ions [8], streptavidin [9–12], neurotransmitters [13], cytokines [14], and chiral organic compounds [15], just to mention a few examples. These papers clearly demonstrate the actual possibility of utilising EGOFETs for the fabrication of robust and sensitive sensors.

The EGOFET device and corresponding sensor performances are universally described using the same basic equations that are traditionally employed to depict the operation of solid-state dielectric-gated O/metal-oxide-semiconductor field-effect transistors (MOSFETs), which are given below [16]:

$$I_{\mathrm{D}} = \frac{W}{L} C_{\mathrm{TOT}} \mu \left(V_{\mathrm{GS}} - V_{\mathrm{TH}}\right) V_{\mathrm{DS}} \tag{1}$$

$$I_{\mathrm{D-SAT}} = \frac{W}{2L} C_{\mathrm{TOT}} \mu \left(V_{\mathrm{GS}} - V_{\mathrm{TH}}\right)^2 \tag{2}$$

where I_{D} is the current flowing between the source and drain electrodes, W is the channel width, L is the channel length, C_{TOT} is the total gate-semiconductor capacitance per unit area, μ is the mobility of the charge carriers, V_{DS} is the drain-source voltage, V_{GS} is the gate-source voltage and V_{TH} is the threshold voltage (i.e. the minimum gate voltage necessary to induce the formation of a conductive path between source and drain) [17]. The two aforementioned equations make a distinction between two different regimes [18, 19]:

(a) for ‘small’ V_{DS} values, the transistors output current I_{D} depends linearly on V_{DS} (linear regime).
(b) when V_{DS} increases, I_{D} reaches an ideally constant (i.e. not depending anymore on V_{DS}) value, called saturation current $I_{\mathrm{D\text{-}SAT}}$ (saturation regime).

Historically, equations (1) and (2) have been developed to describe the electrical behaviour of silicon-based MOSFETs [20] in terms of current–voltage characteristics. In the early years of the organic transistors era [21], these equations have been adopted to fit the transfer and output curves of OFETs and, over the course of the years, they have been adapted to take into account the different phenomena [22], such as contact resistances [23], effects of channel length [24], and especially gate-voltage dependence of mobility [25, 26], introducing deviations from the ideal, expected shapes thus leading to more accurate but also quite complicated analytical models.

Independently of the complexity, these modified MOSFET models usually describe the charge accumulation at the semiconductor/dielectric interface by using a simple parallel-plate capacitor [27] where the compartment between the two ‘plates’ (i.e. the gate electrode and the organic semiconductor) is represented by a solid dielectric. This structure is rather different from that of the EGOFET structure, in which the gate electrode/organic semiconductor capacitive coupling is ensured through the electrolyte characterised by mobile ionic charges, an ion transporting medium and the formation of EDLs [6]. This fundamental difference does have an impact on the analytical models used to describe the operation of EGOFETs in terms of current–voltage curves and thus becomes particularly important when one extracts critical device parameters (such as threshold voltage, charge mobility, and more) necessary to characterise the performances of EGOFETs and EGOFET-based sensors [28].

During recent years, several analytical models of organic devices have been reported attempting to account for the above-mentioned differences. Tu *et al* [3] simulated the two EDLs formed at the gate/electrolyte and electrolyte/semiconductor interfaces as two interfacial series capacitors describing the fact that redistribution of ions inside the electrolyte, upon gate polarisation, is balanced by oppositely charged electronic charge carriers at the gate surface and along the semiconductor surface. This equivalent circuit was then used to develop an EGOFET dc static model in which contact and short-channel effects were also taken into account. Kergoat *et al* [17] later used the same model to elucidate the correlation between the gate metal work function and the transistors threshold voltage. Palazzo *et al* [10] further refined this model by including a third series capacitor associated to the Gouy–Chapman diffuse double layers, which then provides a better description of the electric potential drop within the liquid electrolyte bulk. Another useful and complementary approach take use of electrochemical impedance spectroscopy (EIS) to characterise the total gate/organic semiconductor impedance and then fitting the experimental curves with an equivalent electrical circuit [29, 30]. This approach allows for the identification and estimation of parameters such as the electrolyte resistance and the charge transfer resistance of the redox processes involved.

The above-mentioned approaches provide extremely useful insight on the physical behaviour of EGOFETs but they can often only be used *a posteriori* after that electrical characterisation is completed, to obtain a phenomenological explanation of what has been experimentally observed. Applying these approaches as predictive tools to further advance the field of EGOFETs in general is therefore quite limited.

Within this context, a numerical approach based on the Nernst-Planck-Poisson equations could strongly contribute to the understanding of the physical and operational phenomena of the EGOFETs and provide an accurate description of their experimental behaviour in terms of current–voltage curves and parameters. Additional benefits of this approach include the possibility of generating a spatial map of the physical response of the system at any location, the relatively low-cost investment and the rapid calculation time for the large majority of applications [31]. Recently, such an

approach was successfully used for the description of the polymer-electrolyte blends and organic electrochemical transistors [32, 33]. Surprisingly, the number of reports describing the Nernst-Planck-Poisson analysis of EGOFETs is very limited [5, 34]. Melzer *et al* [5] fabricated organic dual-gate field-effect transistors using poly(3-hexylthiophene) (P3HT) as organic semiconductor. Measurements were carried out by applying two independent gate potentials: one to the back gate, separated from the semiconductor by a thin SiO_2 layer, and the other one to the top gate, an electrode dipped inside an electrolytic solution contacting the P3HT. This strategy allowed for the measurement of the total top gate/organic semiconductor EDLs capacitance. The authors then performed a finite element method simulation of the top-gate EGOFET devices, but the electrolyte was taken into account as an insulating layer between the electrolyte-gate contact and the organic semiconductor region, with a constant capacitance value extracted from the dual gate measurements. A similar model, published by Popescu *et al* [34], was also used to analyse the response of EGOFET-based biosensors for varying bias conditions and ion concentrations in the electrolyte.

In the present paper the Nernst-Planck-Poisson model of the Electrolyte-Gated Field-Effect Transistors (EGOFETs) is developed treating both the polymer and the electrolyte regions of the device on the equal footing. This model is intended to be a very first step towards the construction of more accurate and comprehensive models; for this reason, at this first stage, rather ideal conditions were taken into account (i.e.: absence of charge traps in the semiconductor's bulk and at the semiconductor/electrolyte interface, absence of leakage current between the source and gate electrodes). The model is applied to describe the electrical behaviour of EGOFETs and a semi-quantitative agreement between experimentally measured and calculated output curves and transfer characteristics was found. To the best of our knowledge, this is the first time that an EGOFET model is proposed utilizing the Nernst-Planck-Poisson equations to describe, on equal footing, both the polymer and the electrolyte regions of the device configuration.

Even at this first, idealized stage, we wanted to verify the potential of the model as a predictive tool; to do so, simulations were performed to forecast the influence of a geometrical parameter (i.e. the gate electrode area) on the transistors' electrical behaviour. It is demonstrated computationally and well verified experimentally that EGOFETs with a smaller gate do not exhibit a proper transistor action. The developed model is independent of the choice of material as the organic semiconductor or electrolyte and can be easily adapted for geometries other than those studied here.

The next steps of our work will consist in refining the present model to take into account the aforementioned non-ideal phenomena, to ensure a better correspondence between simulated and experimental curves. Ideally, the final model will allow the user to perform a double task:

(a) on the one hand, it will allow a qualitative description of the transistor's electrical behaviour on the basis of the device geometry and physicochemical parameters of the materials chosen for its fabrication. Under this point of view, the model will be used as a predicting tool, meaning that it will enable the user to qualitatively predict the transistor's electrical behaviour with no actual need for fabricating and measuring the device. The main goal here is to use the model to select the best possible device architecture and materials before moving to the actual fabrication step;
(b) on the other hand, the final model will allow the extraction of the 'macroscopic' figures of merit of the device (namely: I_{ON}/I_{OFF} ratio, subthreshold swing and threshold voltage) by fitting the experimental curves measured on actual devices.

The results of these next steps will be presented in a forthcoming paper.

2. Experimental setup and computational modelling

2.1. EGOFETs fabrication and electrical characterisation

The procedure for the transistors fabrication and characterisation has already been described elsewhere [35, 36]. All solvents were purchased from Sigma-Aldrich and used without further purification. Poly([2,5-bis(3-hexadecyl thiophen-2-yl)thieno[3,2-b]thiophene] (PBTTT-C_{16}) was purchased from Ossila Ltd Transistors were fabricated on p-type silicon wafers covered with a thin SiO_2 layer. The interdigitated source and drain electrodes were realised (see figure 1. Three-dimensional scheme of the EGOFET experimentally studied in this paper) by standard clean-room techniques (Au, $W/L = 30\,000$ μm/10 μm). The organic semiconductor was dissolved in 1,2—dichlorobenzene (5 mg ml^{-1} at 100 °C), deposited by spin-coating (4000 rpm for 180 s, acceleration of 600 rpm s^{-1}) for 180 s and then annealed in air (hot plate, 110 °C, 60 s). The gold gate electrodes were fabricated by using freshly polished gold wires with different diameters, sealed in a glass tube. A PDMS well (3 × 3 mm) was fixed on each transistor and filled with standard phosphate buffer saline solution (pH = 7.4, 0.01 M Na_2HPO_4, 0.0018 M KH_2PO_4, 0.0027 M KCl and 0.137 M NaCl). A schematic view of the device is presented in figure 1. Three-dimensional scheme of the EGOFET experimentally studied in this paper.

Transistors were characterised in terms of output and transfer characteristics using a semiconductor parameter analyser (Keithley 4200 SCS, Keithley Instruments, Germany). The output characteristics ($I_D - V_{DS}$) were recorded by applying different gate voltages (V_{GS}) from $V_{GS} = +0.2$ V to $V_{GS} = -0.6$ V and by sweeping the drain voltage (V_{DS}) between 0 and −0.6 V. The transfer curves ($I_D - V_{GS}$) were recorded by keeping the drain voltage constant at $V_{DS} = -0.4$ V and by sweeping V_{GS} between +0.2 and −0.6 V. In either case, no influence of the scan rate was observed.

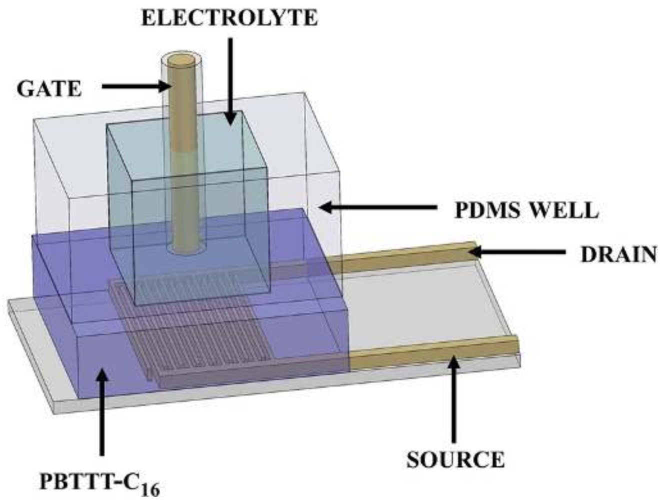

Figure 1. Three-dimensional scheme of the EGOFET experimentally studied in this paper.

2.2. Model

In order to model the electrical behaviour, we need to choose the geometry able to best simulate the experimental EGOFET configuration. The fabricated three-dimensional EGOFET is thus approximated by a two-dimensional (2D) model geometry, see figure 2, which consists of two regions, namely the electrolyte and the organic semiconductor, and the electrodes: source, drain and the gate. The width of the device in the z-direction is 30 000 μm. The multiple interdigitated source and drain electrodes are modelled as six pairs of electrodes of the size of 10 μm separated by 10 μm (corresponding to the dimensions and geometry of actual devices), see figure 2. The gate electrode is capped by an insulating layer (glass) leaving only the metallic bottom exposed to the electrolyte. In this study we considered two gate sizes, namely the large and the small gate having a size of 1.3 μm and 0.3×10^{-3} μm, respectively. These sizes are chosen to represent the actual experimental gate sizes (200 μm and 10 μm in diameter, respectively). These values are re-scaled to account for the fact that the impact of the gate scales with the gate area, and our calculations are performed in a 2D geometry as opposed to the (3D) geometry of the experiments. (Details of re-scaling are provided in SI in section S1 available online at stacks.iop.org/JPD/54/415101/mmedia).

The simulation model is based on the Nernst-Planck-Poisson equations that account for the electrostatics of the system as well as the transport of all the charged species involved. All the equations for the different domains as well as detailed information on the boundary conditions involved in the model are denoted in figure 2, where the organic semiconductor and electrolyte domains are electrically and ionically conductive, respectively.

Hole transport in the organic semiconductor region is described by equation (3) where the flux accounts for both diffusion (first term) and drift (second term) contributions coupled with the Poisson equation (equation (5) describing the electrostatic potential throughout the whole system. The changes in hole concentrations are governed by the continuity equation (equation (4)).

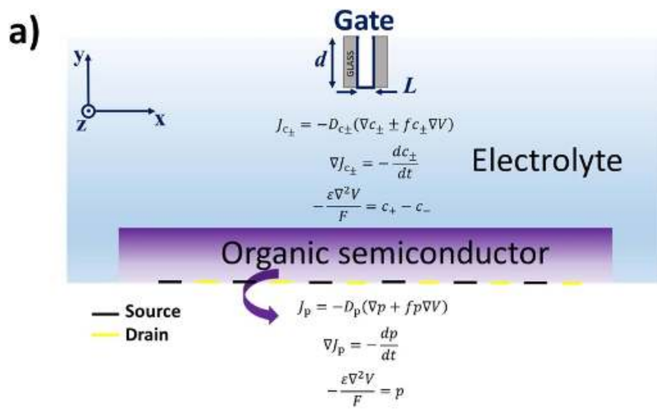

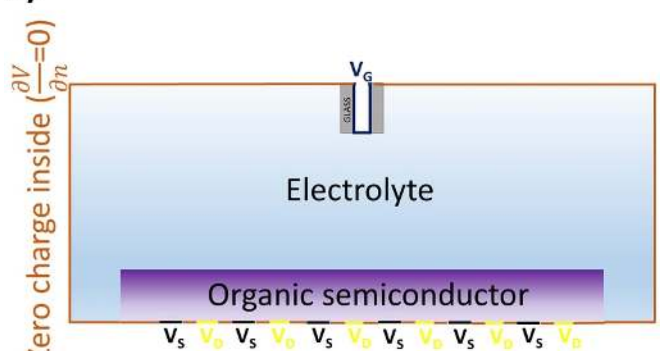

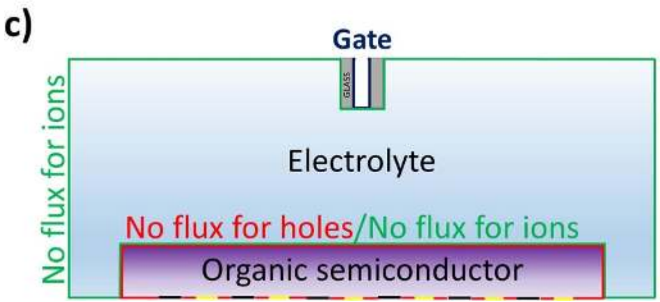

Figure 2. Geometry and equations used in the EGOFET simulations (a). Boundary conditions for the potential (b) and boundary conditions for ions in the electrolyte and holes in the semiconductor region (c).

$$J_{\mathrm{p}} = -D_{\mathrm{p}}\left(\nabla p + fp\nabla V\right) \tag{3}$$

$$\nabla J_{\mathrm{p}} = -\frac{\mathrm{d}p}{\mathrm{d}t} \tag{4}$$

$$-\frac{\varepsilon \nabla^2 V}{F} = p \tag{5}$$

where p and D_{p} are the concentration and diffusion coefficient for holes respectively, J_{p} is the flux of holes and $f = F/RT$ (F the Faraday constant, R the ideal gas constant,

T the temperature), and V the electrostatic potential within the entire system. Similarly, the ion transport in the electrolyte is described by the Nernst-Planck-Poisson equations considering positive and negative ions as the charged species in the electrolytic medium,

$$J_{c_\pm} = -D_{c\pm}\left(\nabla c_\pm \pm f c_\pm \nabla V\right) \tag{6}$$

$$\nabla J_{c_\pm} = -\frac{\mathrm{d}c_\pm}{\mathrm{d}t} \tag{7}$$

$$-\frac{\varepsilon\nabla^2 V}{F} = c_+ - c_- \tag{8}$$

where $c_\pm$ and $D_{c\pm}$ are the concentration and corresponding diffusion coefficients for the cations (+) and anions (−), respectively.

The boundary conditions are applied as follows: for the electric potential, in the semiconductor region the source is grounded, and drain voltage is applied to the drain contact (see figure 2(b)). The gate potential is applied to the gate electrode. All outer boundary conditions except for source, drain and gate correspond to the zero charge inside the device region ($\frac{\partial V}{\partial n} = 0$). Since ions in the electrolyte do not penetrate into the organic semiconductor region, the electrolyte-semiconductor boundary is blocking for both ions and holes. The boundary condition for the hole concentration at the source and drain contacts, n_S and n_D, that accounts for the applied voltage is as follows [37]:

$$n_\mathrm{S} = n_0;\ n_\mathrm{D} = n_\mathrm{S}\exp\left(-\frac{eV_\mathrm{DS}}{kT}\right) \tag{9}$$

where n_0 is a constant, V_DS is the drain voltage, e the elementary charge and k is the Boltzmann constant. (It is noteworthy that for the present system we performed calculations with a simplified boundary condition, $n_\mathrm{S} = n_\mathrm{D}$, and found that it gives practically the same result because of the low concentration of charge carriers).

The boundary condition for ions in the electrolyte region (figure 2(c)) deserves a special discussion. One option is a condition of no flux because the ions cannot leave the electrolyte region [32]. Another boundary condition commonly used in literature is a fixed ion concentration at the boundary [38]. A justification for the latter is that for a large enough electrolyte region the ion concentration at its boundary remains constant and is not affected by the ion re-distribution in the electrolyte region. We performed calculations for both boundary conditions, and we found that the latter (condition of the fixed ion concentration) can lead to unphysical solutions. In particular, we found that under this boundary condition the calculated output and transfer curves are unaffected by the gate size, which clearly contradicts with the experimental observations (see section S2 and figures S1, S2 for details). This arises because the fixed ion concentration boundary condition leads to unphysical solutions with the imbalance between the number of cations and anions in the electrolyte, which violates the overall charge neutrality requirement for the electrolyte (see figure S2(a)). Note that the condition of fixed ion concentration can be used for both stationary and time-dependent simulations. In contrast, the no flux boundary condition cannot be used for the stationary calculations because the ion concentration remains undefined. With that being said, we conclude that the proper EGOFET description should be based on the time-dependent calculations using the condition of no-flux at the boundaries for the electrolyte and defining initial condition for concentration of ions at $t = 0$, that is, $c_\pm\ (t = 0) = c_0$, with c_0 being a constant.

According to the classical model applied to the organic field-effect transistors, equation (1) is used for calculation of the drain current. This equation is based on Ohm's law and completely neglects the diffusion. It also neglects channel shortening due to the pinch-off [39]. In our model, the drain current is calculated on the basis of the drift-diffusion equation (equation (3)), where the current density is the sum of drift and diffusion contributions corresponding to the migration of the charge carriers in an electric field and the flux due to concentration gradient, respectively. The mobility μ is related to the diffusion coefficient by the Nernst-Einstein relation: $\mu_\mathrm{p} = \frac{D_\mathrm{p}}{RT}$. In order to further utilize the potential applicability of our proposed model, we also account for the electric field dependence of the hole mobility. According to the Poole–Frenkel model [40], the mobility dependence on the applied source-drain voltage V_SD is:

$$\mu = \mu_\mathrm{p}\exp\left(\frac{\gamma\sqrt{E}}{kT}\right) \tag{10}$$

where γ is the Poole–Frenkel constant and E is the electric field, which is calculated as $E = V_\mathrm{SD}/d_\mathrm{SD}$, with d_SD being the distance between the source and drain gates. Note that in organic devices the mobility can also depend on the gate voltage, V_GS. To account for this effect, a dependence of μ_p on V_GS can be introduced in equation (10), such that the fitting to the experiment can be easily performed by varying μ_p at a given V_GS to obtain the mobility gate voltage dependence, $\mu_\mathrm{p} = \mu_\mathrm{p}(V_\mathrm{GS})$. In the present study, to keep our model simple, we will treat μ_p as a constant (i.e. gate voltage independent).

The drain current is calculated by integrating the flux of charge carriers over the length of the drain contact: $I_\mathrm{D} = W\int_0^l J_\mathrm{p}\cdot dl$; where W is the channel width. The initial parameters used in the simulations are listed in table 1. Note that the diffusion coefficient for holes for different devices was adjusted in order to fit the experimental and simulated output curves as indicated in the captions to figures 3 and 4. Also, note that the hole concentration reported in the table refers to the pristine semiconductor at room temperature.

In the present study, the EGOFET is simulated using COMSOL Multiphysics 5.5. To perform the calculations, Electrostatics and transport of diluted species modules were coupled as implemented in the software. A corresponding COMSOL file is attached in a supplementary information. The model was performed in 2D with a proper meshing strategy where a very fine mesh was defined at the boundaries of interest e.g. the interface between the electrolyte/organic semiconductor, near the electrodes and a coarser mesh at domains as in the bulk electrolyte (see figure S3 for representative examples).

Table 1. Simulation initial parameters.

Expression	Value
Length of each source/drain contact	10 μm
Semiconductor thickness	300 nm
Semiconductor width (W)	30 000 μm
Large gate size, L (see figure 2(a))	1.3 μm
Small gate size, L (see figure 2(a))	3 nm
Gate extension, d (see figure 2(a))	40 μm
Electrolyte dimensions	370 $\times$ 150 μm
Temperature	300 K
Diffusion coefficient of cations [41]	13.34 $\times$ 10^{-10} m^2 s^{-1}
Diffusion coefficient of anions [41]	20.3 $\times$ 10^{-10} m^2 s^{-1}
Hole concentration (n_0) [42, 43]	10^{-6} mol m^{-3}
Electrolyte concentration	0.1 mol m^{-3}
Dielectric constant of the electrolyte [44]	81
Dielectric constant of the organic semiconductor [45]	2
Poole–Frenkel constant, γ [46]	(2.2–22) $\times$ 10^{-10} E-24 $\left(\frac{m}{V}\right)^{\frac{1}{2}}$ J

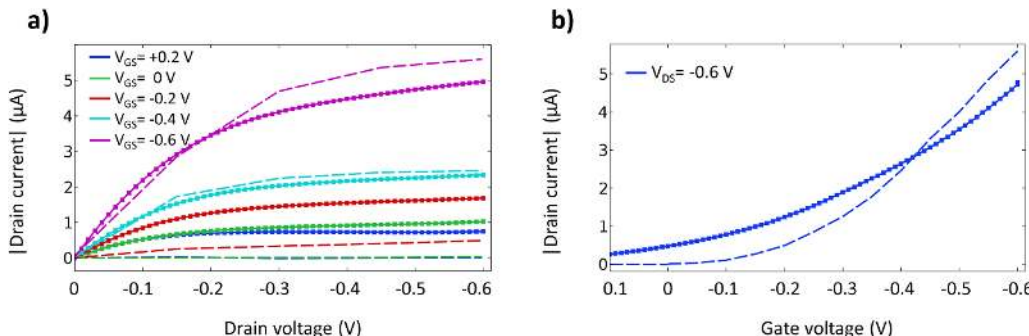

Figure 3. Device characteristics. (a) Experimental (dots with solid lines) and simulated (dashed lines) output curves. (b) Experimental (dots with solid lines) and simulated (dashed lines) transfer curves (currents -hole currents going from the source to the drain- are negative). Diffusion coefficient of holes used in the simulation $D_p = 1.2926 \times 10^{-6}$ m^2 s^{-1}.

3. Results and discussions

3.1. Device electrical analysis

Here, we report the typical current–voltage characteristics of the EGOFET: the transfer and output curves. The output curve is obtained by sweeping the drain voltage and measuring the corresponding drain current whereas the gate voltage is fixed, see figure 3(a). The general trend of the output curve is such that by increasing the drain voltage, the drain current also increases linearly (linear regime). When the drain voltage competes with the effective gate voltage the current evolution starts to reach a plateau (the saturation regime). The transfer characteristics are obtained by performing a parametric sweep on the gate voltage, while the drain voltage is set at a constant value. The resulting transfer curve is shown in figure 3(b). The transfer curve shows typical p-type field-effect characteristics (where the device performs upon negative gate voltage and negative drain voltage and the drain current increases by increasing the gate voltage) [39]. Note that we also calculated output curves accounting for the field dependence of the mobility on the basis of the Poole–Frenkel model, using typical values of the parameter γ (equation (10) and table 1), see figure S4. We found that for the given parameters of the device, the best fit is obtained for the case of the field-independent mobility, i.e. when the mobility does not depend on the applied bias V_{SD}.

It should be noted (see figures S5 and S6 SI) that the transfer curve shows small hysteresis and the gate current is always several orders of magnitude smaller than the drain current (for the same V_{GS} and V_{DS}). For these reasons, we can rule out any relevant electrochemical reactions at both the gate/electrolyte and electrolyte/semiconductor interfaces [7, 47] .

As can be seen from figure 3, the simulated curves are capable to provide a semi-quantitative description of the experimental behaviour; in particular, the simulated output curves reproduce the regions of the linear and saturation regimes. It should be noted, however, that strong differences can be appreciated between the simulated and experimental curves. As can be seen from the transfer curves (figure 3(b)), for more positive gate voltages ($V_{GS} > -0.4$ V) the experimental current is higher (in absolute value) than the simulated current while for more negative gate voltages ($V_{GS} < -0.4$ V) it is the other way round. This observation is consistent with what one can notice on the output curves (figure 3(a)) where, for ($V_{GS} > -0.4$ V) the experimental saturation current is higher (in absolute value) than the simulated saturation current (it is the opposite for $V_{GS} < -0.4$ V) We attribute these

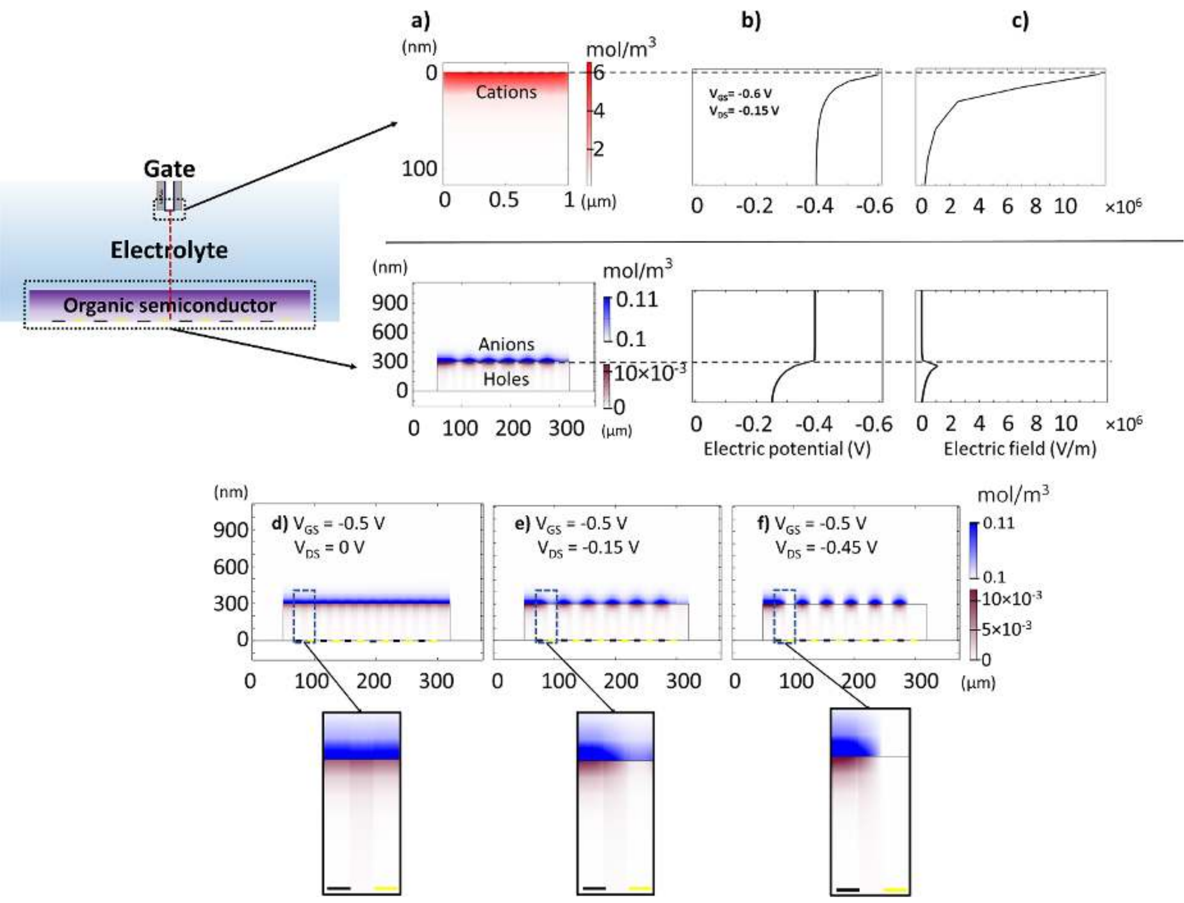

Figure 4. (a) Concentration profiles showing the formation of the electric double layers (cations at the gate and anions at the electrolyte/polymer interface) leading to accumulation of the holes in the channel. (b) The potential profile and (c) the electric field in the *y*-direction (along the cross-section of the device marked by a red dashed line in (a)). A zoomed view on the polymer-electrolyte interface: (d)-(f) the density of anions (blue) and holes (dark purple) for different drain voltages.

differences to the fact that in real devices, charge carriers' density and mobility are not constants but it does depend on the gate voltage V_{GS}; more in detail, it has been shown that for polythiophene-based semiconductors mobility increases for small gate voltages, then saturates and finally decreases for higher gate voltages [20]. This behaviour seems consistent with the observations made on the transfer curves. Another aspect that can be observed when comparing the experimental output and transfer curves is that, for the same V_{GS} and V_{DS} values, currents in the transfer curves do not perfectly correspond to those of the output curves. This difference can be tentatively attributed to the experimental protocol used for the acquisition of the output curves. During the acquisition of the first output curves, the device is polarised for several seconds by applying positive gate voltages; in the case of transfer curves, the duration of positive gate biasing is much shorter (a few tens of ms). It has been shown that the prolonged application of positive gate voltages to p-type transistors typically results in a shift of the threshold voltage towards more positive values [48]; in polythiopene-based systems, this phenomenon is usually attributed to the injection by the drain and source contacts of electrons at the organic semiconductor/dielectric interface; these negative charges are trapped at the interface, even when the gate voltage is shifted towards negative values, and are responsible for the accumulation of holes in the transistor's channel. As a consequence, the absolute value of the threshold voltage is reduced [49].

Herein, we bring the concentration and potential profiles into focus and discuss the formation of electric double layers and charge carrier profiles inside the device. In a p-channel device, upon negative polarisation of the gate, the associated electric field alters the distribution of ions in the electrolyte, such that cations are attracted towards the gate/electrolyte interface, while anions migrate to the electrolyte/polymer interface leaving the bulk electrolyte charge-neutral (p-type operation). Thus, as expected, the formation of the electric double layers at both interfaces is observed. This leads to accumulation of holes in the polymer region where a conducting channel is formed at the nanometre distance next to the interface, figure 4(a). The potential profile at the cross-section of the device is shown in figure 4(b). Since there is no charge left in the bulk electrolyte, the potential is constant there (because the flat potential corresponds to no charge). The electric field which is the driving force for ion migration is therefore zero in the bulk of the electrolyte, and it is high where the EDLs are formed, i.e. at the gate/electrolyte and electrolyte/polymer interfaces.

Let us now discuss the hole density across the channel for different drain voltages. At low drain voltages $|V_{DS}|$, charge carriers are distributed rather uniformly at the polymer/electrolyte interface between the source and drain electrodes (see figure 4(d)). As a result, the transistor obeys Ohm's law when the current increases linearly with raising the drain voltage. This is referred to as the linear regime [19]. When the magnitude of the drain voltage $|V_{DS}|$ is increased, the concentration gradient along the polymer/electrolyte is introduced and the concentration of the charge carriers is reduced to zero at the drain contact because of the combined action of the drain electrode and the top gate, see figure 4(e). The transistor therefore enters the pinch-off regime. When the drain voltage increases even more the depletion region near the drain electrode grows, leading to shortening the channel length, see figure 4(f). In this case the transistor operates in the saturation regime when an increase of the drain voltage does not lead to further increase of the drain current beyond the saturation level. The saturation of the current is the result of two competing effects, the growth of the depleted region near the drain electrode (favoring the decrease of the current) and the increase of $|V_{DS}|$ (favoring the increase of the current). Finally, we would like to point out that while this behaviour was qualitatively well understood before, our calculations present the actual density distributions of ions and holes as well as the electric field and potential profiles directly calculated from the Nernst-Planck and Poisson equations.

3.2. Effect of the gate size on device performance

In this section we investigate and analyse the electrical response of the EGOFET with the small gate, in an aim to test our model and to further understand the limiting boundaries of the EGOFETs. The measured output characteristics are shown in figure 5(a) (plotted as solid lines). In contrast to the case of a large gate, the EGOFET with the small gate does not show any transistor action (i.e. the dependence of the drain current on the applied gate voltage), c.f. figures 3(a) and 5(a). The simulated output characteristics are shown in figure 5(a) in the form of dots. While the calculated dependencies still exhibit some field effect, it is much less pronounced in comparison to the case of the large gate, c.f. figures 3(a) and 5(a). For example, for the same drain voltage $V_D = -0.5$ V, the relative change of the current with the change of V_{SG} from $V_{SG} = 0$ V to $V_{SG} = -0.6$ V is $|I_{-0.6V} - I_{0V}|/I_{0V} \approx 20$ for the case of the large gate, and $|I_{-0.6V} - I_{0V}|/I_{0V} \approx 3$ for the case of the small gate. Note that similar behaviour of the EGOFETs with a varying ratio between the size of the gate and the semiconductor channel was reported by White *et al* [50] for the EGOFETs with a floating gate.

It is noteworthy that the measured current for the case of a small gate is two orders of magnitude smaller as compared to the case of the large gate. This reflects the fact that the small gate induces much lower hole concentration in the polymer. It is interesting that for the case of the large gate the calculated and the measured current are comparable in magnitude, whereas for the small-gate EGOFET the measured current is much lower than the calculated one. We speculate that this can be due to the fact that in the polymer at low hole density many hole percolative paths through the device can be blocked due to the effect of the impurities confining the charge carriers in isolated space regions [51, 52].

In order to understand the absence of the field effect for the case of a small gate, we analyse the distribution of charges and formation of the double layers in the system at hand, see figures 5(b)–(d). For the case of the EGOFET with a small gate, the potential mostly drops across the gate–electrolyte interface, where the electric field is high, whereas the voltage drops at the polymer/electrolyte interface and the electric field there are negligible, see figures 5(c) and (d). This is in contrast to the case of the EGOFET including a large gate area, where the voltage drops at the gate-electrolyte and at the polymer–electrolyte interface are comparable in magnitude, c.f. figures 4(b) and 5(c). The reason why the potential drop on the small gate is much higher than on the large one, can be explained by the text-book electrostatics prescribing that the electric field near a surface is inversely proportional to the surface curvature. Indeed, whereas the large gate can be considered as essentially flat, small gates can be regarded as point-like sources giving rise to circular symmetric fields, c.f. potential profiles in figures 4(a) and 5(b) for the small and large gates, respectively. Alternatively, this can be easily understood by considering the gate–electrolyte interface and the electrolyte–polymer interface as two series connected capacitors. Because the former has much smaller area than the latter, the voltage drop occurs at primarily at the gate–electrolyte interface.

The large potential drop at the gate and the high value of the electrical field there for the case of the small gate leads to the enhanced screening of the gate by cations (the gate being negatively polarised here). As a result, the EDL at the gate presents a much higher charge density as compared to the EDL at the polymer/electrolyte interface, see figure 5(b). In other words, the EDL at this second interface is practically absent. This means that the gate does not practically induce and affects the density of holes in the polymer, which results in the absence of the transistor action. In contrast, for the case of EGOFET with the large gate, two EDLs are formed and a variation of the gate voltage results in the modulation of the hole density in the EDL polymer/electrolyte interface leading to the effective transistor action.

It is noteworthy that the efficiency of the gate screening depends on the concentration of the electrolyte. We performed calculation of the electrical characteristics of the EGOFET for the case of the electrolyte with much lower concentration, corresponding to the ionized water with $c = 10^{-4}$ mol m^{-3}. In this case, as expected, the gate is poorly screened, and the transistor action is partially restored, see figure S7.

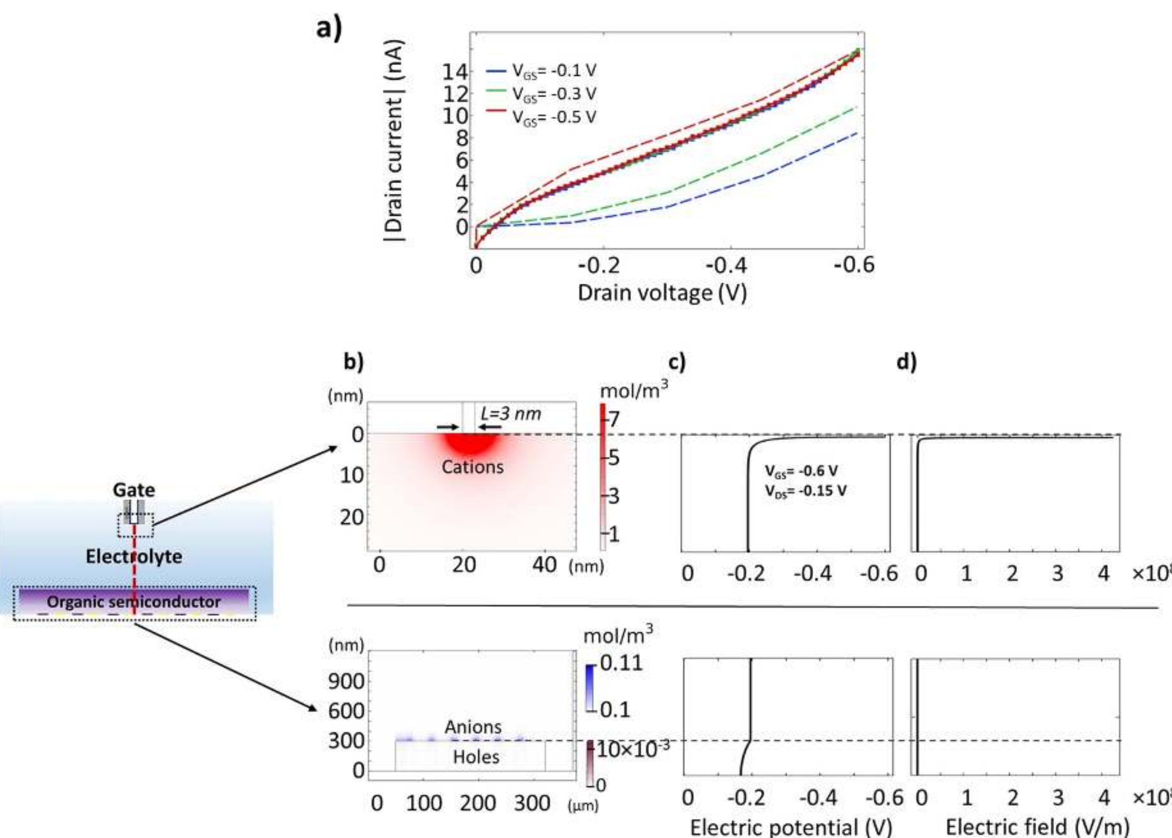

Figure 5. Electrical characterization of the EGOFET with small gate. (a) experimentally measured (dots with solid lines) and calculated (dashed lines) output characteristics (currents-hole currents going from the source to the drain- are negative). (b) Concentration profile showing the higher concentration of cations at the gate, screening the small gate more effectively. (c) Potential profile and (d) electric field plot in y-direction. Diffusion coefficient of holes used in the simulation $D_p = 2.5852 \times 10^{-8}$ m^2 s^{-1}.

4. Conclusion

In the present study a model of the electrolyte–gated organic field-effect transistors based on the Nernst-Planck-Poisson equations was developed. This model treats both the polymer and the electrolyte regions of the device on an equal footing. This allows for an accurate quantitative description of the electrical characteristics of EGOFETs of an arbitrary geometry. Additional benefits of this approach are to produce a spatial map of the physical response of the system at any location, such as electron and ion concentration, electric potential, and electric field distribution.

The experimentally measured current–voltage characteristics (the output and transfer curves) were modelled and analysed using the developed model, and semi-qualitative agreement between the experimental and calculated results was found. Based on the developed model, various regimes of the EGOFET operation (i.e. linear, pinch-off and saturation) were discussed and analysed using the calculated concentration and potential profiles and the formation of electric double layers inside the device.

To practically test our model, simulations were performed to forecast the influence of a geometrical parameter such as the gate electrode area on the transistors' electrical behaviour. We showed, both experimentally and via simulations, that the performance of the EGOFET strongly depends on the gate size. In particular, the device with a small gate does not exhibit a transistor action (i.e. the dependence of the drain current on the applied gate voltage). We demonstrated that this happens because the electric potential for the case of the small gate drops primarily at the gate/electrolyte interface, which results in the high concentration of cations at this interface shielding the electric field generated by the gate. As a result, the double layer does not form at the electrolyte/polymer interface, and the EGOFET no longer performs as a transistor.

Our results also outline one technical aspect of the simulation that is important for the accurate description of the organic devices operating in aqueous environment using the Nernst-Planck-Poisson. Namely, we demonstrated that the steady-state approach utilising the boundary conditions corresponding to the fixed electrolyte concentration at the boundary can lead to unphysical solutions causing the ion imbalance inside the device violating the overall charge neutrality requirement. Hence, we conclude that an accurate description of EGOFETs requires time-dependent simulations using the condition of no-flux for the ions at the boundaries of the electrolyte and defining initial condition for the concentration of ions at $t = 0$.

Altogether, we believe that our study demonstrates that our Nernst-Planck-Poisson-based model can be successfully used for qualitative description of EGOFETs electric behaviour. To further improve agreement between simulated and experimental results and to be finally able to use this model both

as a predictive tool and as a tool for macroscopic figures of merit extraction from experimental curves, non-ideal phenomena have to be taken into account; this will be the object of a forthcoming paper.

Data availability

All data that support the findings of this study are included within the article (and any supplementary files).

Acknowledgments

This work was supported by the Swedish Research Council (Project 2017-04474). K T thanks the Swedish Government Strategic Research Area in Materials Science on Advanced Functional Materials at Linköping University (Faculty Grant SFO-Mat-LiU No. 2009-00971) for support. The computations were performed on resources provided by the Swedish National Infrastructure for Computing (SNIC) at NSC and HPC2N. This work was also funded by the French National Research Agency (Agence Nationale de la Recherche) through the project EGOFLEX ANR-17-CE08-0025.

ORCID iDs

Najmeh Delavari https://orcid.org/0000-0002-6098-991X
Klas Tybrandt https://orcid.org/0000-0002-9845-446X
Magnus Berggren https://orcid.org/0000-0001-5154-0291
Benoît Piro https://orcid.org/0000-0003-2874-5824
Vincent Noël https://orcid.org/0000-0003-3901-8358
Giorgio Mattana https://orcid.org/0000-0003-0552-3970
Igor Zozoulenko https://orcid.org/0000-0002-6078-3006

References

[1] Kergoat L, Herlogsson L, Braga D, Piro B, Pham M C, Crispin X, Berggren M and Horowitz G 2010 A water-gate organic field-effect transistor *Adv. Mater.* **22** 2565–9
[2] Sonmez B G, Ertop O and Mutlu S 2017 Modelling and realization of a water-gated field effect transistor (WG-FET) using 16 nm thick mono-Si film *Sci. Rep.* **7** 1–8
[3] Tu D, Herlogsson L, Kergoat L, Crispin X, Berggren M and Forchheimer R 2011 A static model for electrolyte-gated organic field-effect transistors *IEEE Trans. Electron Devices* **58** 3574–82
[4] Braga D and Horowitz G 2009 High-performance organic field-effect transistors *Adv. Mater.* **21** 1473–86
[5] Melzer K, Brändlein M, Popescu B, Popescu D, Lugli P and Scarpa G 2014 Characterization and simulation of electrolyte-gated organic field-effect transistors *Faraday Discuss.* **174** 399–411
[6] Wang D, Noël V and Piro B 2016 Electrolytic gated organic field-effect transistors for application in biosensors—a review *Electronics* **5** 9
[7] Kergoat L, Piro B, Berggren M, Pham M C, Yassar A and Horowitz G 2012 DNA detection with a water-gated organic field-effect transistor *Org. Electron.* **13** 1–6
[8] Schmoltner K, Kofler J, Klug A and List-Kratochvil E J 2013 Electrolyte-gated organic field-effect transistor for selective reversible ion detection *Adv. Mater.* **25** 6895–9
[9] Magliulo M, Mallardi A, Mulla M Y, Cotrone S, Pistillo B R, Favia P, Vikholm-Lundin I, Palazzo G and Torsi L 2013 Electrolyte-gated organic field-effect transistor sensors based on supported biotinylated phospholipid bilayer *Adv. Mater.* **25** 2090–4
[10] Palazzo G, De Tullio D, Magliulo M, Mallardi A, Intranuovo F, Mulla M Y, Favia P, Vikholm-Lundin I and Torsi L 2015 Detection beyond debye's length with an electrolyte-gated organic field-effect transistor *Adv. Mater.* **27** 911–6
[11] Mulla M, Seshadri P, Torsi L, Manoli K, Mallardi A, Ditaranto N, Santacroce M, Di Franco C, Scamarcio G and Magliulo M 2015 UV crosslinked poly (acrylic acid): a simple method to bio-functionalize electrolyte-gated OFET biosensors *J. Mater. Chem.* B **3** 5049–57
[12] Suspène C, Piro B, Reisberg S, Pham M C, Toss H, Berggren M, Yassar A and Horowitz G 2013 Copolythiophene-based water-gated organic field-effect transistors for biosensing *J. Mater. Chem.* B **1** 2090–7
[13] Casalini S, Leonardi F, Cramer T and Biscarini F 2013 Organic field-effect transistor for label-free dopamine sensing *Org. Electron.* **14** 156–63
[14] Casalini S, Dumitru A C, Leonardi F, Bortolotti C A, Herruzo E T, Campana A, De Oliveira R F, Cramer T, Garcia R and Biscarini F 2015 Multiscale sensing of antibody–antigen interactions by organic transistors and single-molecule force spectroscopy *ACS Nano* **9** 5051–62
[15] Mulla M Y, Tuccori E, Magliulo M, Lattanzi G, Palazzo G, Persaud K and Torsi L 2015 Capacitance-modulated transistor detects odorant binding protein chiral interactions *Nat. Commun.* **6** 1–9
[16] Macchia E, Picca R A, Manoli K, Di Franco C, Blasi D, Sarcina L, Ditaranto N, Cioffi N, Österbacka R and Scamarcio G 2020 About the amplification factors in organic bioelectronic sensors *Mater. Horiz.* **7** 999–1013
[17] Kergoat L, Herlogsson L, Piro B, Pham M C, Horowitz G, Crispin X and Berggren M 2012 Tuning the threshold voltage in electrolyte-gated organic field-effect transistors *Proc. Natl Acad. Sci.* **109** 8394–9
[18] Cramer T, Kyndiah A, Murgia M, Leonardi F, Casalini S and Biscarini F 2012 Double layer capacitance measured by organic field effect transistor operated in water *Appl. Phys. Lett.* **100** 86
[19] Lamport Z A, Haneef H F, Anand S, Waldrip M and Jurchescu O D 2018 Tutorial: organic field-effect transistors: materials, structure and operation *J. Appl. Phys.* **124** 071101
[20] Bourguiga R, Mahdouani M, Mansouri S and Horowitz G 2007 Extracting parameters from the current-voltage characteristics of polycrystalline octithiophene thin film field-effect transistors *Eur. Phys. J. Appl. Phys.* **39** 7–16
[21] Horowitz G 1998 Organic field-effect transistors *Adv. Mater.* **10** 365–77
[22] Sworakowski J 2015 Current–voltage characteristics in organic field-effect transistors. Effect of interface dipoles *Chem. Phys.* **456** 106–10
[23] Kim C H and Horowitz G 2019 Toward a fully analytical contact resistance expression in organic transistors *Materials* **12** 1169
[24] Mittal P, Kumar B, Negi Y S, Kaushik B K and Singh R 2012 Channel length variation effect on performance parameters of organic field effect transistors *Microelectron. J.* **43** 985–94
[25] Schliewe R, Yildirim F, Von Emden W, Witte R, Bauhofer W and Krautschneider W 2006 Static model for organic

field-effect transistors including both gate-voltage-dependent mobility and depletion effect *Appl. Phys. Lett.* **88** 233514
[26] Jung S, Jin J W, Mosser V, Bonnassieux Y and Horowitz G 2019 A compact model and parameter extraction method for a staggered OFET with power-law contact resistance and mobility *IEEE Trans. Electron Devices* **66** 4894–900
[27] Un H I, Wang J Y and Pei J 2019 Recent efforts in understanding and improving the nonideal behaviors of organic field-effect transistors *Adv. Sci.* **6** 1900375
[28] Dumitru L M, Manoli K, Magliulo M, Sabbatini L, Palazzo G and Torsi L 2013 Plain poly (acrylic acid) gated organic field-effect transistors on a flexible substrate *ACS Appl. Mater. Interfaces* **5** 10819–23
[29] Porrazzo R, Bellani S, Luzio A, Lanzarini E, Caironi M and Antognazza M R 2014 Improving mobility and electrochemical stability of a water-gated polymer field-effect transistor *Org. Electron.* **15** 2126–34
[30] Piro B, Wang D, Benaoudia D, Tibaldi A, Anquetin G, Noël V, Reisberg S, Mattana G and Jackson B 2017 Versatile transduction scheme based on electrolyte-gated organic field-effect transistor used as immunoassay readout system *Biosens. Bioelectron.* **92** 215–20
[31] Rao S S 2005 *The Finite Element Method in Engineering* (Oxford: Butterworth-Heinemann, Elsevier) pp 3–43
[32] Volkov A V, Wijeratne K, Mitraka E, Ail U, Zhao D, Tybrandt K, Andreasen J W, Berggren M, Crispin X and Zozoulenko I V 2017 Understanding the capacitance of PEDOT: PSS *Adv. Funct. Mater.* **27** 1700329
[33] Tybrandt K, Zozoulenko I V and Berggren M 2017 Chemical potential–electric double layer coupling in conjugated polymer–polyelectrolyte blends *Sci. Adv.* **3** eaao3659
[34] Popescu D, Popescu B, Brändlein M, Melzer K and Lugli P 2015 Modeling of electrolyte-gated organic thin-film transistors for sensing applications *IEEE Trans. Electron Devices* **62** 4206–12
[35] Fillaud L, Petenzi T, Pallu J, Piro B, Mattana G and Noel V 2018 Switchable hydrogel-gated organic field-effect transistors *Langmuir* **34** 3686–93
[36] Tibaldi A, Fillaud L, Anquetin G, Woytasik M, Zrig S, Piro B, Mattana G and Noël V 2019 Electrolyte-gated organic field-effect transistors (EGOFETs) as complementary tools to electrochemistry for the study of surface processes *Electrochem. Commun.* **98** 43–46
[37] Bartesaghi D, Van Der Kaap N and Koster L J A 2016 3D simulations of organic solar cells *Unconventional Thin Film Photovoltaics* (Cambridge: Royal Society of Chemistry) pp 420–52
[38] Szymański M Z, Tu D and Forchheimer R 2017 2D drift-diffusion simulation of organic electrochemical transistors *IEEE Trans. Electron Devices* **64** 5114–20
[39] Köhler A and Bässler H 2015 *Electronic Processes in Organic Semiconductors: An Introduction* (New York: Wiley)
[40] Gill W 1972 Drift mobilities in amorphous charge-transfer complexes of trinitrofluorenone and poly-n-vinylcarbazole *J. Appl. Phys.* **43** 5033–40
[41] Lide D R and Kehiaian H V 1994 *CRC Handbook of Thermophysical and Thermochemical Data* (Boca Raton, FL: CRC Press)
[42] Cochran J E, Junk M J, Glaudell A M, Miller P L, Cowart J S, Toney M F, Hawker C J, Chmelka B F and Chabinyc M L 2014 Molecular interactions and ordering in electrically doped polymers: blends of PBTTT and F4TCNQ *Macromolecules* **47** 6836–46
[43] Kang K, Watanabe S, Broch K, Sepe A, Brown A, Nasrallah I, Nikolka M, Fei Z, Heeney M and Matsumoto D 2016 2D coherent charge transport in highly ordered conducting polymers doped by solid state diffusion *Nat. Mater.* **15** 896–902
[44] Archer D G and Wang P 1990 The dielectric constant of water and Debye-Hückel limiting law slopes *J. Phys. Chem. Ref. Data* **19** 371–411
[45] Hughes M P, Rosenthal K D, Ran N A, Seifrid M, Bazan G C and Nguyen T Q 2018 Determining the dielectric constants of organic photovoltaic materials using impedance spectroscopy *Adv. Funct. Mater.* **28** 1801542
[46] Blom P W, De Jong M and Van Munster M 1997 Electric-field and temperature dependence of the hole mobility in poly (p-phenylene vinylene) *Phys. Rev.* B **55** R656
[47] Picca R A, Manoli K, Macchia E, Tricase A, Di Franco C, Scamarcio G, Cioffi N and Torsi L 2019 A study on the stability of water-gated organic field-effect-transistors based on a commercial p-type polymer *Front. Chem.* **7** 667
[48] Sirringhaus H 2009 Reliability of organic field-effect transistors *Adv. Mater.* **21** 3859–73
[49] Chua L L, Zaumseil J, Chang J F, Ou E C W, Ho P K H, Sirringhaus H and Friend R H 2005 General observation of n-type field-effect behaviour in organic semiconductors *Nature* **434** 194–9
[50] White S P, Dorfman K D and Frisbie C D 2016 Operating and sensing mechanism of electrolyte-gated transistors with floating gates: building a platform for amplified biodetection *J. Phys. Chem.* C **120** 108–17
[51] Ihnatsenka S, Crispin X and Zozoulenko I 2015 Understanding hopping transport and thermoelectric properties of conducting polymers *Phys. Rev.* B **92** 035201
[52] Jido D and Kanada-En'yo Y 2008 K K^- N molecule state with I = 1/2 and J P = 1/2+ studied with a three-body calculation *Phys. Rev.* C **78** 035203